THE JOURNAL OF PHYSICAL CHEMISTRY A

Article

pubs.acs.org/JPCA

Monte Carlo–Quantum Mechanics Study of Magnetic Properties of Hydrogen Peroxide in Liquid Water

María Cristina Caputo,*[,†] Patricio F. Provasi,[‡] Lucía Benitez,[‡] Herbert C. Georg,[§] Sylvio Canuto,[¶] and Kaline Coutinho[¶]

[†]Departamento de Física, FCEN, UBA and IFIBA, Conicet, Ciudad Universitaria, 1428, Buenos Aires, Argentina

[‡]Department of Physics - IMIT, Northeastern University, Av. Libertad 5500, Corrientes, Argentina

[§]Instituto de Física, Universidade Federal de Goiás, CP 131, 74001-970 Goiânia, GO, Brazil

[¶]Instituto de Física, Universidade de São Paulo, CP 66318, 05315-970 São Paulo, Brazil

ABSTRACT: A theoretical study of magnetic properties of hydrogen peroxide in water has been carried out by means of Monte Carlo simulation and quantum mechanics calculations. The solvent effects were evaluated in supermolecular structures generated by simulations in the *NPT* ensemble. The solute–solvent structure was analyzed in terms of radial distribution functions, and the solute–solvent hydrogen bonds were identified with geometric and energetic criteria. Approximately three water molecules are hydrogen bonded to H_2O_2 (0.6 and 0.8 in each hydrogen and oxygen atom, respectively, of the H_2O_2). Although, on average, both hydroxyls of the peroxide are equivalent, the distribution of hydrogen-bonded water molecules is highly asymmetric. Analyzing the statistics of the hydrogen bonds, we identify that only 34% of the configurations give symmetric distributions around the two hydroxyls of the H_2O_2 simultaneously. The magnetic shieldings and the indirect spin–spin coupling constants were calculated at the B3LYP/aug-cc-pVTZ and aug-cc-pVTZ-J computational level. We find that the solvent shields the oxygen and unshields the hydrogen atoms of the peroxide (+5.5 and −2.9 ppm, respectively), with large fluctuation from configuration to configuration in the oxygen case, an effect largely accounted for in terms of a single hydrogen bond with H_2O_2 as the proton donor. The most sensitive coupling in the presence of the solvent is observed to be the one-bond J(O,H).

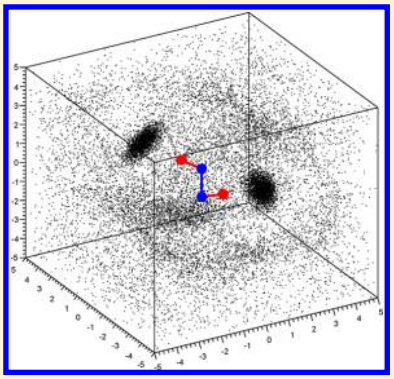

1. INTRODUCTION

Hydrogen peroxide, H_2O_2, is an oxidizing and bactericide compound whose chemical reactions confer on it an important role in natural phenomena and industrial processes. All of these reactions require a medium, which is mostly water, where H_2O_2 forms hydrogen-bonded complexes whose study comprises an important subdomain of hydrogen peroxide chemistry (see, for instance, Kulkarni[1] and references therein). From the molecular theoretical standpoint, this has prompted a number of works dedicated to study small $H_2O_2\cdots(H_2O)_n$ complexes. Xue-Hai et al.[2] investigated the structures, IR shifts, binding energies, and thermodynamic properties of such a complex for $n = 1-3$ clusters with ab initio methods, while Kulkarni et al.,[1] performed extensive quantum chemical analyses on these complexes for $n = 1-6$ with Hartree–Fock (HF) method and second-order Møller–Plesset perturbation theory (MP2), studying the effect of clustering by water molecules on the vibrational frequencies and providing a tool to understand the cooperative effects and the structural changes in small clusters. Ferreira et al.[3] studied the electronic excitation and the ionization energy of hydrogen peroxide–water clusters with $n = 1-6$ using density functional theory (B3LYP) for the geometries and time-dependent density functional theory (TDDFT) and equation of motion coupled cluster with single and double excitations (EOM-CCSD).

Several calculations of structural and electronic properties of H_2O_2 in water have been reported using dielectric continuum models.[4−9,32] However, computer simulations of H_2O_2 in aqueous solution are scant. As far as we know, there are only two works that performed molecular dynamics simulations in a multiscale quantum mechanics/molecular mechanics (QM/MM) approach to investigate the energetic and structural properties of H_2O_2 in water.[10,38] None of them study the NMR properties of the H_2O_2 in solution, although the description and the understanding of the role played by the environment in the NMR properties is essential to help in the elucidation of biological macromolecule structures. In this framework, the purpose of this paper is to analyze the effects of the aqueous solvation in the NMR properties of hydrogen peroxide.

Solvation effects in NMR properties are generally taken into account using two best-proven approaches, the continuum model of the medium, involving the quantum chemical consideration of a single molecule surrounded by a continuous homogeneous dielectric medium, and the supermolecule model, where intermolecular complexes composed of the molecule under consideration and several solvent molecules interacting with it are explicitly calculated.

Received: November 17, 2013
Revised: July 18, 2014
Published: July 21, 2014

QM/MM methods, a version of the supermolecule approach where the spatial arrangement of the solvent molecules around the molecule under study is set by classical Monte Carlo (MC) simulation or molecular dynamics methods, are, in particular, employed for problems involving hydrogen bonds (HBs) between the solute and the solvent[11] as the one considered in this work, where the dielectric approximation is not adequate.

In particular, for the calculation of NMR properties in liquid water, several QM/MM variations have been followed: a hybrid method[12] with an additional short-ranged repulsive potential that pushes the electrons out of regions that would be occupied by neighboring electrons of the surrounding classical atoms; the inclusion of explicit microscopic polarization effects[13] by assigning to each solvent molecule an electric dipole polarizability and thus giving rise to instantaneous induced dipole moments in the solvent; or a completely quantum approach, where the dynamically fluctuating hydrogen-bond network is taken into account explicitly in generating configurations,[14,15] the method of choice particularly when the solvation effects lead to changes in solute geometry and electronic structure.

In the present work, we study the influence of water on the NMR properties of hydrogen peroxide, following a QM/MM approach with a classical mechanics Hamiltonian described by force fields. Special attention is paid to the role played by HBs between the solute and the solvent. We take fixed molecular geometries and investigate separately the validity of this approximation.

2. COMPUTATIONAL DETAILS

Quantum mechanical (QM) calculations of the magnetic properties of H_2O_2 were performed for the isolated solute molecule (S) and in aqueous solution (S + solvent), where the solvent was described by the polarizable continuum model (PCM)[16] and by an explicit model with and without electrostatic embedding (nW + PC and nW, respectively).[17,18] This discrete model of the solvent was composed by n water molecules explicitly included in the QM calculations, where n varied from 1 to 6. Additionally, an electrostatic embedding was also used, composed of the atomic point charges of the remaining water molecules of the solution. The positions of the water molecules around the H_2O_2 were obtained from configurations generated by MC simulations. Therefore, the magnetic properties, such as magnetic shieldings and coupling constants (SSCC), were calculated and averaged for the H_2O_2 in aqueous solution using several models, S + PCM (solute + polarizable continuum model), S + nW (solute + n explicit water molecules), and S + nW + PC (solute + n explicit water molecules + electrostatic embedding described by atomic point charges) with n = 1, 2, 3, and 6, and compared with S (isolated solute in vacuum). All of the QM NMR calculations were performed with the GIAO[19] methods in the GAUSSIAN program[20] using density functional theory with the B3LYP exchange−correlation.[21,22] A systematic study[23] of SSCC calculations with core−valence bases of incremental size with the DFT-B3LYP, RPA, and SOPPA methods showed that the former has better convergence.

Four basis sets of increasing quality were tested to investigate the minimal size sufficient for our calculations, aug-cc-pVDZ, aug-cc-pVTZ, aug-cc-pVQZ, and aug-cc-pV5Z,[24] with, respectively, 64, 138, 252, and 414 basis functions for H_2O_2 and 41, 92, 172, and 287 basis functions for water. From the results shown in section 3.2, we chose to employ the aug-cc-pVTZ set as it is within 10% of the HF limit and still of manageable size for the QM calculation of magnetic properties with explicit treatment of neighboring solvent molecules.

The above basis sets have been developed to describe with flexibility the valence region of the electronic system and are therefore not adequate to describe the electron density in the vicinity of the nucleus, as needed for SSCC calculations.[25] Thus, special basis sets with core functions, which take into account the electronic correlation with participation of inner electrons, are of major importance for the atoms between which SSCCs are calculated, in particular, for the contribution due to the Fermi contact (FC) interaction.[26] In this work, we use the aug-cc-pVTZ-J set,[27−30] a contracted correlation-consistent triply split polarized-diffuse basis set specially optimized for calculations of second-order properties by contracting the aug-cc-pVTZ basis set, with the most diffused functions excluded and four 1s-contracted tight s functions added for all elements.

Metropolis MC simulations were performed in the isothermal−isobaric *NPT* ensemble using standard procedures.[31] We used periodic boundary conditions and the image method in a cubic box whose initial volume was determined by the experimental density ρ = 0.997 g/cm^3. The system was composed of one solute molecule of H_2O_2 embedded in 300 solvent molecules of water in the room conditions (T = 298 K and P = 1 atm). The hydrogen peroxide and the water molecules interact by the Lennard-Jones plus Coulomb potential, with three parameters for each interacting site (ϵ_i, σ_i, and q_i). These parameters were taken from the work by Vácha et al.[32] for hydrogen peroxide and from the work by Jorgensen[33] for water. This election is motivated by preliminary studies showing that it gives reasonable structural and thermodynamic descriptions of the liquid water at room temperature and that our results do not depend heavily on the water model used.

The simulations were performed with the DICE program.[34] It involves a thermalization stage of about 1.5 × 10^6 MC steps followed by an averaging stage of 3.0 × 10^6 MC steps. The average density was calculated as 0.99 ± 0.01 g/cm^3, in agreement with the result for liquid water.

The geometry used for the water molecule corresponds to intramolecular distances of r_{OH} = 0.970 Å and r_{HH} = 1.55 Å,[35] and for the peroxide molecule, we referred to the geometry of complex II of the article by Xue-Hai et al.,[2] r_{HO} = 0.983 Å, r_{OO} = 1.475 Å with angles θ_{HOO} = 98.2°, ϕ_{HOOH} = 115.1°. This geometry is similar to the experimental one obtained by Redington et al.[36] During the simulations, the geometry of the molecules is kept rigid.

In reality, it is not possible to make a full QM calculation of the magnetic properties of the supermolecular system composed of 300 molecules over thousands of MC steps. Alternatively, after the simulation, we sample 100 configurations with less than 11% of statistical correlation, evaluated using the correlation function method as discussed in ref 37, and perform our QM calculation using only a few selected number of solvent molecules. Therefore, the value of the magnetic properties is thus obtained by an ensemble average over the statistically uncorrelated structures generated in the simulations. As a further verification of the proper statistical treatment of the solvated system, the full simulation was subdivided into 10 samples of 10 contiguous configurations each. Calculations of magnetic properties give identical results for each sample within the statistical uncertainties, and a χ^2 test of independence yields χ^2/ndf = 9.31/9, confirming that the configurations are sufficiently uncorrelated.

dx.doi.org/10.1021/jp411303n | J. Phys. Chem. A 2014, 118, 6239−6247

This procedure reduces dramatically the number of configuration used in the QM calculations when compared with the entire number of MC steps.

For each one of the 100 statistically uncorrelated configurations, several supermolecular structures are considered, $H_2O_2 + (H_2O)_n$, where n is the number of water molecules hydrogen bonded to H_2O_2 (n = 1, 2, and 3) and the first microsolvation shell (n = 6). The NMR properties were calculated for these supermolecular structures bare and embedded with the electrostatic field of the remaining water molecules of the solution.

3. RESULTS

3.1. Solvation Shell and Hydrogen Bonds. The solvation shells are obtained from the radial distribution function (RDF) between the center of mass of H_2O_2 and water molecules, $G_{CM-CM}(r)$, shown in Figure 1a. In this $G_{CM-CM}(r)$, it is easy to notice the formation of a sharp peak from 2.6 to 3.7 Å, which describes a microsolvation shell composed of the HBs. The complete first solvation shell goes up to 5.0 Å. The number of water molecules, $N(r)$, is obtained by the spherical integration of the $G_{CM-CM}(r)$ until a distance r; see Figure 1b. Then, 6 water molecules are found in the microsolvation shell and 17 in the entire first solvation shell.

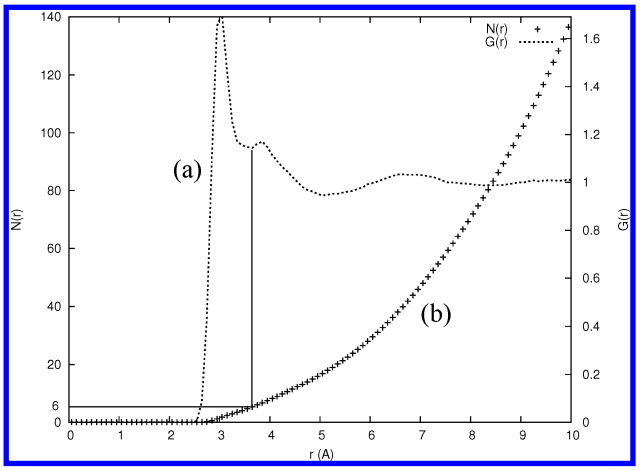

Figure 1. (a) The RDF between the center of mass of H_2O_2 and water molecules, $G_{CM-CM}(r)$, and (b) its spherical integration, $N(r)$.

An important aspect in the solvation of H_2O_2 in water is the formation of HBs. Hydrogen-bonded structures are conventionally obtained from the analysis of the RDFs $G_{O-H}(r)$ and $G_{H-O}(r)$. These distributions are shown in Figure 2a, $G_{O_s-H_w}(r)$ between the oxygen atoms of the solute H_2O_2 and the water hydrogen atoms and $G_{H_s-O_w}(r)$ between the hydrogen atoms of the solute H_2O_2 and the water oxygen atoms. For comparison, the water distribution $G_{H-O}(r)$ is superimposed in each case in Figure 2b. The first peak of the $G_{H_s-O_w}(r)$ (Figure 2, left), associated with the solute−solvent HBs, is more intense and appears at a shorter distance (by 0.06 Å) for H_2O_2 than that for water. However, their integrations, up to 2.5 Å, give approximately the same coordination number of 2.0 for both distributions (one HB per hydrogen atom of H_2O_2 and of water). Therefore, the HBs formed by the hydrogen atoms of H_2O_2 are more structured than those formed by the hydrogen atoms of water, and this is an indication of the well-known fact that H_2O_2 is a better proton donor than water, in agreement with ref 38. This larger structuralization of the water molecules hydrogen bonded to the H_2O_2 can be seen in the three-dimensional distribution of the center of mass of the water molecules as two dense clouds near each hydrogen atom of the H_2O_2 (see Figure 3). However, in the opposite situation is the first peak of the $G_{O_s-H_w}(r)$ (Figure 2, right) which is less intense and appears at a larger distance (by 0.24 Å) for H_2O_2 than that for water. Their integrations, up to 2.5 Å, give the coordination number of approximately 1.4 for each oxygen atom of the H_2O_2 and 1.9 for the oxygen of water. In the inset of $G_{O_s-H_w}(r)$, the distribution of the two nearest hydrogen atoms of water composing its first peak is shown. It is clear that by integrating up to the first minimum, each oxygen atom of the H_2O_2 has less than two water molecules hydrogen bonded, and therefore, the oxygen atom in the molecule of H_2O_2 is a poorer proton acceptor than the water molecule.

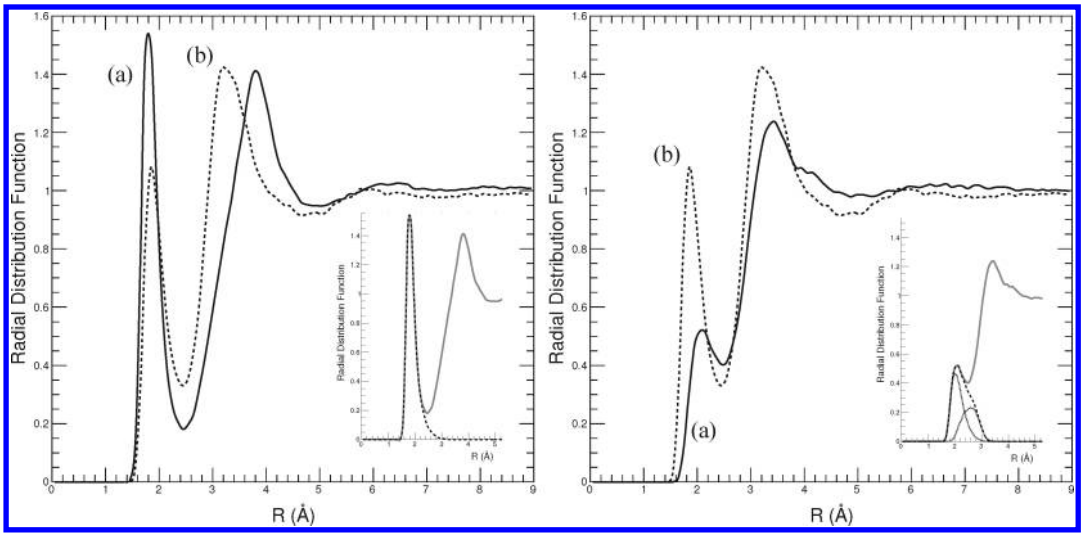

Figure 2. RDFs for H_2O_2 in aqueous solution (solid line) between the hydrogens of H_2O_2 and the water oxygens, $G_{H_s-O_w}(r)$ (left), and between the oxygens of H_2O_2 and the water hydrogens, $G_{O_s-H_w}(r)$ (right). For comparison, the same distributions are shown for liquid water (dotted line). (Insets) (left) The RDF of the closest solvent oxygen atom (dashed line) fully describes the HB peak; (right) the RDFs of the first and second closest hydrogen atoms are shown separately (dotted lines), and their sum (dashed line) describes the HB peak.

dx.doi.org/10.1021/jp411303n | J. Phys. Chem. A 2014, 118, 6239−6247

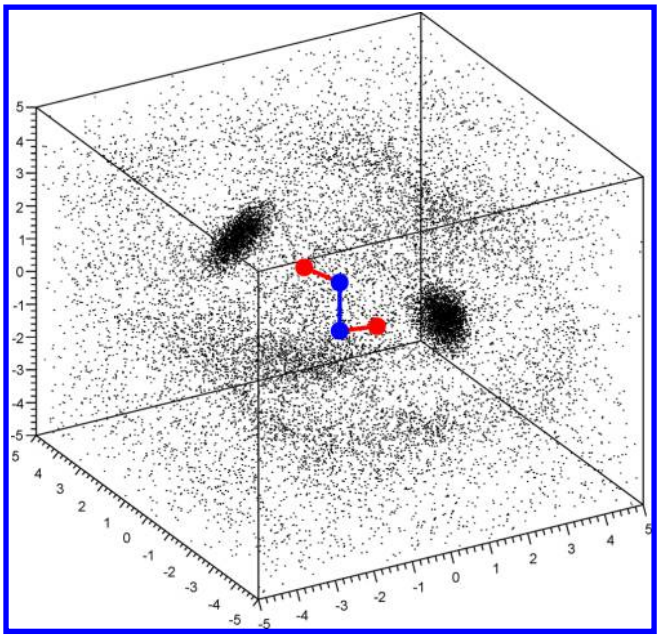

Figure 3. Solvent center of the mass three-dimensional distribution around the solute H_2O_2 molecule: a superposition of the 100 statistically uncorrelated MC configurations in a box of 10 Å edges.

Hence, on the basis of the integration of both distributions, $G_{O_s-H_w}(r)$ and $G_{H_s-O_w}(r)$, the H_2O_2 has, on average, 4.8 HBs with the water molecules.

HBs in liquids are better obtained using geometric and energetic criteria, as discussed before.[39,40] The criteria used here for the HB formation are the distance $R_{O-O} \leq 3.3$ Å, the angle $\Theta_{O-OH} \leq 40°$, and the binding energy higher than 1.6 kcal/mol. In doing so, an average of 2.8 HBs formed between the H_2O_2 and water molecules is found (0.6 in each hydrogen and 0.8 in each oxygen atom of the H_2O_2). Note that this is an average for the solution, but H_2O_2 can form up to six simultaneous HBs with the surrounding water molecules. The statistics obtained for the HBs formed are 9% of the configurations form one HB, 24% form two HBs, 42% form three HBs, and 25% form four HBs.

In summary, when considering the distance between the centers of mass of the H_2O_2 and the H_2O molecules, we observe a first peak in the RDF corresponding to six solvent molecules surrounding the solute, thus defining the microsolvation shell henceforth used for full QM calculations. When restricting to the H−O distances between H_2O_2 and H_2O, we find an average of 4.8 solvent molecules within the HB distance of the solute, and when further imposing stricter angular and binding energy criteria, the average number of H_2O_2−H_2O HBs gets reduced to 2.4. Analyzing the statistics of HBs, we identify that only 34% of the configurations yield symmetric distributions around the hydrogen peroxide, 12% with both hydroxyls acting as proton donor and 22% with both hydroxyls simultaneously acting as the proton donor and acceptor. Therefore, the majority of the configurations (66%) give asymmetric distributions, most of them (42%) with the hydrogen peroxide acting as the proton donor and acceptor in one hydroxyl and proton donor in the other.

3.2. Magnetic Shieldings. In order to assess the influence of solvation on the magnetic shieldings of hydrogen and oxygen for H_2O_2 in water, we perform a full QM treatment of H_2O_2 in vacuum (σ_S) and in water. The aqueous environment is described by four models: (i) when no explicit water molecules were included, the solution was described with PCM (σ_{S+PCM}); (ii) when one water molecule hydrogen bonded was explicitly included (σ_{S+1W}) for special studies; (iii) when the first microsolvation shell, composed of six water molecules (σ_{S+6W}), was explicitly included; and (iv) we also consider the electrostatic field of the remaining water molecules of the solution, including those in the QM calculations as atomic point charges ($\sigma_{S+6W+PC}$). The positions of the solvent molecules are obtained by sampling 100 statistically uncorrelated configurations obtained in the averaging stage of the MC simulation.

Figure 4 shows the oxygen shielding results with basis sets of an increasing number of functions for isolated H_2O_2 and for

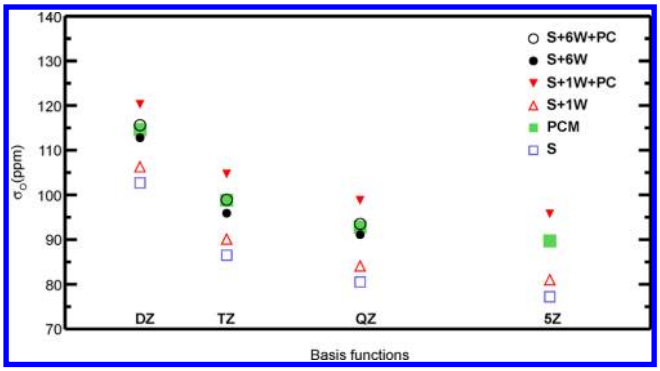

Figure 4. Isotropic magnetic shielding for oxygen in H_2O_2, in ppm, for four sets of basis functions, aug-cc-pVDZ, aug-cc-pVTZ, aug-cc-pVQZ, and aug-cc-pV5Z, as a function of the number of basis functions for H_2O_2, respectively, 64, 138, 252, and 414.

H_2O_2 in water using the four solvation approximations described above. Only one configuration was considered for the σ_{S+1W}, σ_{S+6W}, and $\sigma_{S+6W+PC}$ cases, and the largest base could not be employed for the full first microsolvation shell complexes. It is observed that the basis set used in this work, aug-cc-pVTZ, is within 10% of the limit attained with the largest basis.

The results in Figure 5 show the distribution of results for σ_H and σ_O obtained by QM calculations for the H_2O_2 surrounded by the six nearest water molecules and the remaining ones treated as atomic point charges (S+6W+PC model) at B3LYP/aug-cc-pVTZ. The histograms contain 200 entries, two per configuration, and are well described by Gaussian distribution fits, superimposed on the plot. For comparison, we show the mean shieldings obtained for the isolated solute (σ_S) and in solution described by the continuum model (σ_{S+PCM}) and by the first microsolvation shell (σ_{S+6W}). The results are summarized in Table. 1.

We observe that the distribution for hydrogen is narrow (the standard deviation of the distribution of σ(H) is 1.4 ppm) and that the mean value of σ_H monotonically decreases for the vacuum, PCM, 6W, and 6W + PC models. The values are, in ppm, $\sigma_S = 24.2 > \sigma_{S+PCM} = 22.8 > \sigma_{S+6W} = 21.8 \pm 0.1 > \sigma_{S+6W+PC} = 21.3 \pm 0.1$.

For oxygen, the situation changes; the distribution is an order of magnitude wider (standard deviation of 13.8 ppm), and the values of σ_O follow a different relationship, in ppm, $\sigma_S = 86.5 < \sigma_{S+6W} = 90.6 \pm 1.0 < \sigma_{S+6W+PC} = 92.7 \pm 1.0 < \sigma_{PCM} = 98.8$.

The widespread oxygen shielding values, ranging from 60 to 120 ppm, can be traced back to the fact that in a given solution configuration, the two oxygen atoms in H_2O_2 are not chemically equivalent. This is illustrated by the left panel of Figure 6, which plots the distribution of $\sigma(O_2)$ versus $\sigma(O_1)$, where O_1 and O_2

dx.doi.org/10.1021/jp411303n | J. Phys. Chem. A 2014, 118, 6239−6247

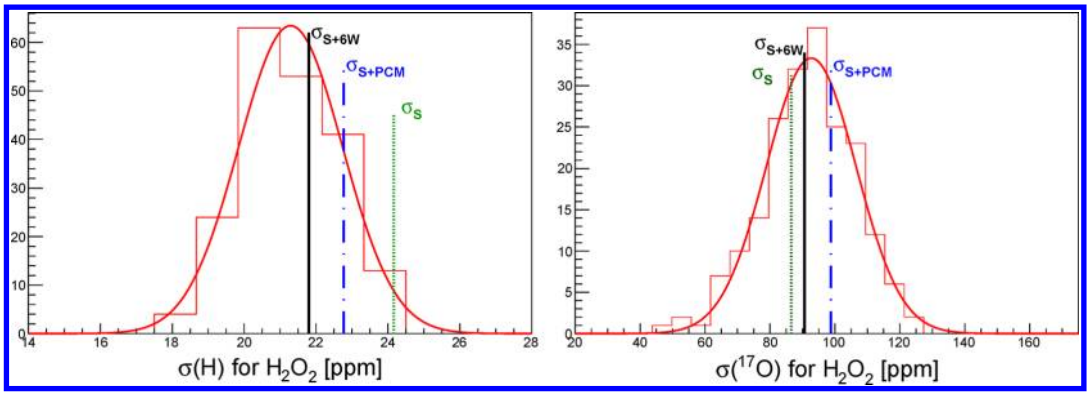

Figure 5. Isotropic magnetic shielding for hydrogen (left) and oxygen (right) for H_2O_2 in water. The solvent is simulated by including in the QM calculation the first microsolvation shell of six water molecules and representing the remaining water molecules by the electrostatic field of their atomic point charges ($\sigma_{S+6W+PC}$). The histogram depicts the distribution of individual results for each configuration, together with a Gaussian fit to the data. For comparison, the mean shielding is shown for three other cases: in vacuum (σ_S), with PCM (σ_{S+PCM}), and with the first microsolvation shell (σ_{S+6W}).

Table 1. Isotropic Magnetic Shieldings in ppm for H_2O_2 in Vacuum (σ_S), in Water with the Continuum Model (σ_{S+PCM}), with the First Microsolvation Shell Explicitly Included (σ_{S+6W}), and with the First Microsolvation Shell Plus Electrostatic Embedding of the Remaining Water Molecules of the Solution ($\sigma_{S+6W+PC}$), at the B3LYP/aug-cc-pVTZ Level[a]

atom	σ_S	σ_{S+PCM}	σ_{S+6W}	$\sigma_{S+6W+PC}$
O	86.5	98.8	90.6 ± 1.0	92.7 ± 1.0
H	24.2	22.8	21.8 ± 0.1	21.3 ± 0.1

[a]For the last two cases, the error of the mean is also indicated.

are the two oxygen atoms (chosen at random) in the H_2O_2 molecule, when including in the QM calculation the first microsolvation shell of six water molecules. A strong negative correlation is observed; the more shielded one nucleus, the less shielded the other one.

Further insight into this shielding/deshielding behavior is gained by studying the magnetic properties of hydrogen peroxide plus one water molecule forming a H_s-O_w bond as a function of the HB distance (d_{HO}), as shown in the right panel of Figure 6. The remote oxygen (open circles) is always shielded, while the nearby oxygen (solid circles) is deshielded; the stronger the effect, the closer the solvent molecule. The complete range of variation observed in the first microsolvation shell treatment is accounted for in terms of a single HB distance. The average of the two shieldings (solid squares) is found to be basically independent of the HB length.

A similar study for the two hydrogen atoms in H_2O_2 shows that in this case, their magnetic shieldings are not correlated; see the left panel in Figure 7. The range covered, from 19 to 24 ppm, is again explained by a single HB to water. This is illustrated in the right panel, which plots the shielding as a function of the HB distance. The hydrogen atom involved in the HB (solid circles) is deshielded down to 19 ppm when the solvent molecule is the closest, while the shielding of the remote one (open circles) is independent of the bond distance, explaining thus the lack of correlation.

The influence of including electrostatic embedding to describe the remaining solution molecules, in addition to the explicit first microsolvation shell, is best studied by considering the sequence $\sigma_S \rightarrow \sigma_{S+6w} \rightarrow \sigma_{S+6w+PC}$, that is, the isolated, first microsolvation shell only and the first microsolvation shell plus atomic point charge shieldings. The oxygen results for $\Delta\sigma_{6w} \equiv \sigma_{S+6w} - \sigma_S$,

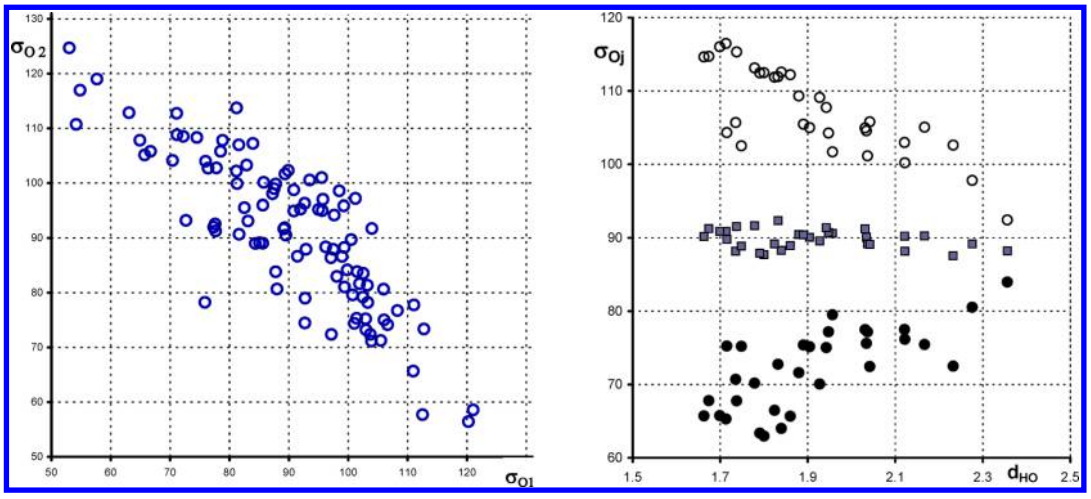

Figure 6. Isotropic magnetic shielding in ppm for oxygen in H_2O_2. (Left) $\sigma(O_2)$ versus $\sigma(O_1)$, the two oxygen atoms in a H_2O_2 molecule, when H_2O_2 is surrounded by the six water molecules of the first microsolvation shell. A strong negative correlation is observed. (Right) $\sigma(O)$ as a function of the HB distance in Å (d_{HO}) for H_2O_2 in the presence of one water molecule forming a HB with H_2O_2 acting as the proton donor. The oxygen atom nearby the HB gets unshielded (solid circles) and the remote one shielded (open circles), while their average stays essentially constant (gray squares).

dx.doi.org/10.1021/jp411303n | J. Phys. Chem. A 2014, 118, 6239−6247

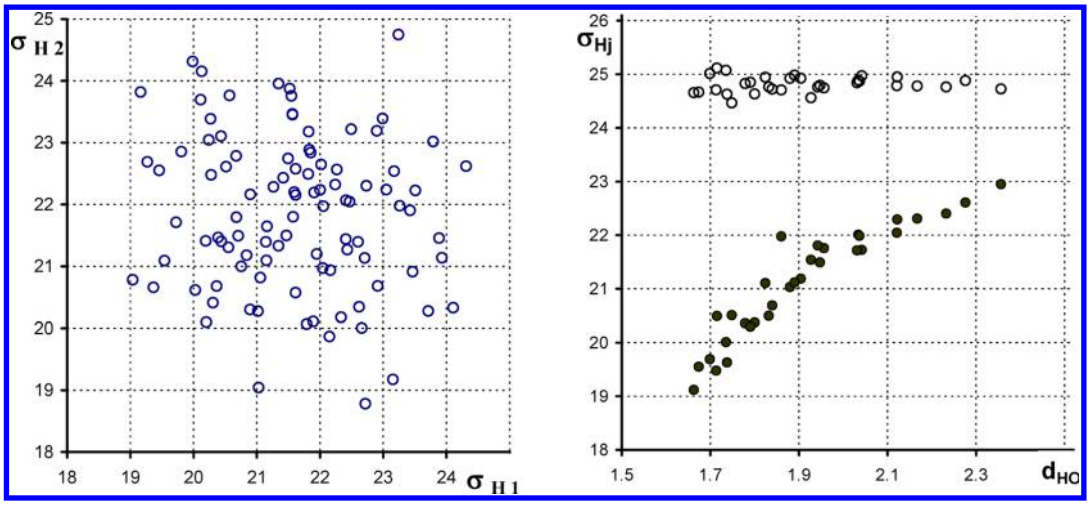

Figure 7. Isotropic magnetic shielding in ppm for hydrogen in H_2O_2. (Left) $\sigma(H_2)$ versus $\sigma(H_1)$: the two hydrogen atoms in a H_2O_2 molecule when H_2O_2 is surrounded by the six water molecules of the first microsolvation shell. No correlation is observed. (Right) σ(H) as a function of the HB distance in Å (d_{HO}) for H_2O_2 in the presence of one water molecule forming a HB with H_2O_2 acting as the proton donor. The hydrogen atom participating in the HB gets unshielded (solid circles), while the remote one is unaffected.

$\Delta\sigma_{PC} \equiv \sigma_{S+6w+PC} - \sigma_{S+6w}$, and $\Delta\sigma \equiv \sigma_{S+6w+PC} - \sigma_S$ are well described by N (average, standard deviation) Gaussian distributions. The results, in ppm, for these distributions are (4.1, 14.0), (1.4, 9.1), and (5.5, 13.9), respectively. The corresponding distributions and Gaussian fits for $\Delta\sigma_{6w}$ and $\Delta\sigma_{PC}$ are shown in Figure 8a and b; those for $\Delta\sigma$ are not included because they overlap with the former.

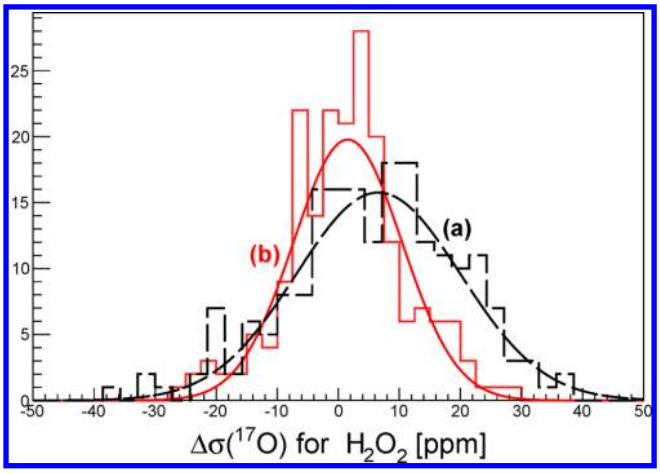

Figure 8. Distribution of $\Delta\sigma(^{17}O)$, the change in the oxygen magnetic shielding for each configuration: (a) Dashed line: H_2O_2 (vacuum) → H_2O_2 (first microsolvation shell); (b) Solid line: H_2O_2 + 6 water (explicit) → H_2O_2 + 6 water (explicit) + electrostatic embedding.

The interpretation of the mean values is straightforward. The +5.5 ppm net solvation shift in $\Delta\sigma_O$ is decomposed as 75% of the effect when including the first microsolvation shell (6W) and 25% when adding the electrostatic embedding (PC). The result for the spread in $\Delta\sigma_O$ is interesting. If the fluctuations in the two steps $\sigma_S \rightarrow \sigma_{S+6w} \rightarrow \sigma_{S+6w+PC}$ were independent, one would expect a global width of $[(14.0)^2 + (9.1)^2]^{1/2} = 16.7$ ppm for $\Delta\sigma$, rather than the observed 13.9 ppm. This implies a certain level of anticorrelation.

The changes in the hydrogen shielding when including solvent effects are shown in Figure 9. The distributions are well described by Gaussian functions, with N (average, standard deviation)

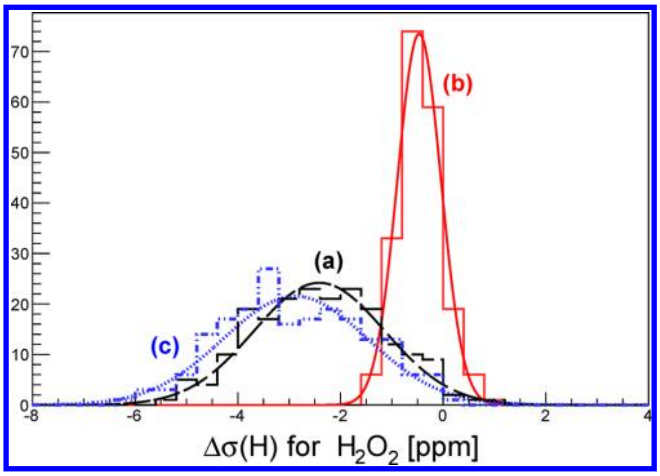

Figure 9. Distribution of $\Delta\sigma$(H), the change in the hydrogen magnetic shielding for each configuration: (a) Dashed line: H_2O_2 (vacuum) → H_2O_2 (first microsolvation shell); (b) Solid line: H_2O_2 + 6 water (explicit) → H_2O_2 + 6 water (explicit) + electrostatic embedding; (c) Dotted line: H_2O_2 (vacuum) → H_2O_2 + first microsolvation shell + electrostatic embedding.

parameters (−2.4, 1.3), (−0.5, 0.4), and (−2.9, 1.4) for $\Delta\sigma_{6W}$, $\Delta\sigma_{PC}$, and $\Delta\sigma$, in Figure 9a−c, respectively. The hydrogen nucleus is deshielded by the solvent, with 85% of the change accounted for by the first microsolvation shell. The additional contribution of the electrostatic field of the remaining solution molecules is small and, contrary to the oxygen case, does not present large fluctuations.

The solvation effects described above correspond to the environmental change brought about by the presence of water molecules around the hydrogen peroxide. Another consequence of solvation, however, is a possible change of the solute geometry itself. In order to assess the relevance of this contribution, we computed the shielding change for reasonable variations of the hydrogen peroxide geometry; see Table 2. For hydrogen, the geometrical effect is an order of magnitude lower than the environmental effect. For oxygen, the geometrical effect is comparable, albeit of opposite sign, to the net shift due to solvation and a factor of 5 smaller than the fluctuations between configurations.

dx.doi.org/10.1021/jp411303n | J. Phys. Chem. A 2014, 118, 6239−6247

Table 2. Shielding Variation, $\Delta\sigma$ (ppm), Produced by Changes in the H_2O_2 Geometry

geometry	change	$\Delta\sigma$(O)	$\Delta\sigma$(H)
dihedral angle	10°	0.40	0.23
angle O−O−H	2°	−4.07	1.03
distance O−H	0.01 Å	−4.3	−0.02
distance O−O	0.005 Å	−4.0	−0.09

Table 3. Intramolecular Spin−Spin Coupling Constants in Hz for Hydrogen Peroxide in Vacuum and in Aqueous Solution

H_2O_2	^1J(O,O)	^1J(O,H)	^2J(O,H)	^3J(H,H)
S	27.67	−42.04	−6.97	0.92
a	5.35	−61.42	−7.75	1.73
b	7.47	−71.25	−7.10	1.52
c	18.13	−60.24		
d	33.07	−64.38		
S + PCM	28.61	−54.50	−6.26	0.66
S + 1W	28.77 ± 1.15	−45.26 ± 4.18	−6.70 ± 0.39	0.83 ± 0.08
S + 1W + PC	30.55 ± 1.60	−53.37 ± 4.40	−6.30 ± 0.38	0.62 ± 0.07
S + 2W	28.51 ± 1.05	−51.98 ± 1.93	−6.27 ± 0.24	0.57 ± 0.08
S + 2W + PC	30.09 ± 1.89	−57.60 ± 3.70	−6.02 ± 0.31	0.44 ± 0.08
S + 3W	29.46 ± 1.69	−49.55 ± 3.19	−6.54 ± 0.39	0.77 ± 0.09
S + 3W + PC	30.67 ± 1.96	−56.88 ± 3.83	−6.17 ± 0.23	0.57 ± 0.09
S + 6W	28.64 ± 1.79	−53.54 ± 4.27	−6.32 ± 0.37	0.62 ± 0.11
S + 6W + PC	29.27 ± 1.82	−56.89 ± 4.57	−6.18 ± 0.40	0.53 ± 0.12

[a]Taken from ref 46 calculated at the B3LYP/aug-pcJ-3 level. [b]Taken from ref 46 calculated at the SOPPA(CCSD)/aug-ccJ-pVQZ level. Both were obtained using the molecular equilibrium geometry optimized at the B3LYP/6-31G* level. [c]Taken from ref 47 calculated at SOPPA/Ahlrichs,[48] using the molecular equilibrium geometry optimized at the MP2/aug-cc-pVTZ level. [d]Taken from ref 47 calculated at SOPPA/Ahlrichs,[48] using the experimental geometry from ref 36.

3.3. Coupling Constants. Within the Ramsey approximation, the total spin−spin coupling constant (J) is a sum of four contributions, the paramagnetic spin−orbit (PSO), diamagnetic spin−orbit (DSO), Fermi contact (FC), and spin dipole (SD).[41,42] The former two account for the interaction between the nuclear spins and the orbital angular momentum of the electrons, whereas the latter two account, respectively, for the interaction between the nuclear and electronic spins and the presence of the electronic spins in the nuclear positions. In Table 3 are gathered all intramolecular coupling constants for hydrogen peroxide at the B3LYP/aug-cc-pVTZ-J level of theory. Comparison of our result with other works shows similar patterns but quantitatively different results from a high sensitivity with the level of calculations and the geometry employed. Unfortunately, we were not able to find any report of experimental results of the intramolecular coupling constants of the hydrogen peroxide for comparison.

The most notorious observation is that the one-bond couplings, ^1J(O,O) and ^1J(O,H), increase in absolute value with the presence of the solvent, whereas the two- and three-bond couplings ^2J(O,H) and ^3J(H,H), decrease. In all cases, the consideration of point charges, in addition to the explicit water molecules, reinforces these changes.

We can see that the tendency observed for the gas−liquid shift of the hydrogen peroxide in this work is ∼−15 Hz for ^1J(O,H); see Table 3. The lack of experimental values for this compound could be substituted meanwhile by the similar coupling constant in water. Thus, we can consider some very good calculations of the gas-phase one-bond coupling ^1J(O,H), which are −77.2[43] and −76.7 Hz.[44] Both values together with the experimental result, −80.6 Hz,[45] which corresponds to the liquid phase, show that the same gas−liquid shift is around −3.4 to −3.9 Hz in the same direction as that for hydrogen peroxide.

As expected, the S + nW and S + nW + PC shift of the calculated coupling constants, that is, $|\Delta^m J(\mathrm{O,X})| = |{}^m J^{\mathrm{S}+n\mathrm{W}+\mathrm{PC}}_{(\mathrm{O,X})} - {}^m J^{\mathrm{S}+n\mathrm{W}}_{(\mathrm{O,X})}|$, diminish with n (the number of water molecules involved) and tend to a unique value.

It is interesting to remark that for all four coupling constants, the S + PCM value is very close to the first microsolvation shell result.

The four contributions to the coupling constants are shown in Table 4. The errors were omitted, and only the averages were considered to facilitate the analysis. The FC contribution is only dominant for the ^1J(O,H) couplings. The liquid−vapor change of ∼1.5 Hz for the ^1J(O,O) coupling arose from the increase in the FC contribution because the SD and PSO almost compensate for each other and the DSO is negligible. The largest liquid−vapor change is ∼14.9 Hz for the ^1J(O,H) coupling and comes mainly from the FC contribution, ∼16.9 Hz, compensated for in ∼2.0 Hz by the PSO one. The ^2J(O,H) couplings show similar orders of magnitude and solvent effects on both contributions, FC and PSO, and they are −0.53 and −0.37 Hz, producing a global change of −0.80 Hz. Finally, the ^3J(H,H) couplings show a liquid−vapor variation of the same order (∼1.0 Hz) but opposite to each other for the PSO and DSO contributions; thus, the small change in the FC (∼0.4 Hz) is the one that determines the global change.

As mentioned in section 3.2, in addition to the environmental change studied above, solvation can produce small variations in the solute geometry itself. This effect can be estimated by

Table 4. Four Contributions to the Intramolecular Spin−Spin Coupling Constants in Hz for Hydrogen Peroxide in Vacuum and in Aqueous Solution

$n H_2O$	^1J(O,O)				^1J(O,H)				^2J(O,H)				^3J(H,H)			
	FC	SD	PSO	DSO	FC	SD	PSO	DSO	FC	SD	PSO	DSO	FC	SD	PSO	DSO
S	−22.15	17.80	31.99	0.03	−40.69	0.35	−1.55	−0.14	−4.19	1.08	−4.09	0.23	1.31	−0.39	4.02	−4.02
S + PCM	−21.37	17.60	32.35	0.04	−54.32	0.34	−0.39	−0.12	−3.71	1.11	−3.90	0.23	1.15	−0.40	3.96	−4.04
S + 1W	−21.34	17.83	32.24	0.04	−44.33	0.36	−1.10	−0.19	−4.01	1.10	−3.99	0.20	1.23	−0.40	3.77	−3.78
S + 1W + PC	−20.14	17.83	32.83	0.04	−53.38	0.36	−0.19	−0.17	−3.72	1.13	−3.90	0.20	1.10	−0.41	3.72	−3.79
S + 2W	−22.50	17.83	33.14	0.04	−52.34	0.29	0.34	−0.27	−3.65	1.12	−3.87	0.13	1.05	−0.42	3.17	−3.22
S + 2W + PC	−21.04	17.76	33.32	0.04	−58.45	0.25	0.86	−0.27	−3.48	1.14	−3.80	0.13	0.95	−0.43	3.13	−3.21
S + 3W	−20.39	17.69	32.11	0.05	−49.06	0.39	−0.64	−0.24	−3.96	1.12	−3.85	0.16	1.19	−0.40	3.53	−3.55
S + 3W + PC	−19.64	17.66	32.60	0.05	−57.25	0.38	0.21	−0.22	−3.70	1.15	−3.77	0.16	1.06	−0.41	3.49	−3.57
S + 6W	−21.70	17.65	32.62	0.06	−53.86	0.27	0.39	−0.34	−3.75	1.13	−3.76	0.07	1.08	−0.42	2.86	−2.90
S + 6W + PC	−20.99	17.56	32.64	0.06	−57.55	0.25	0.75	−0.34	−3.66	1.14	−3.72	0.07	1.02	−0.42	2.83	−2.90

dx.doi.org/10.1021/jp411303n | J. Phys. Chem. A 2014, 118, 6239−6247

re-evaluating the coupling constants for reasonable modifications of the hydrogen peroxide geometry. In particular, we find a change of $\Delta^1J(O,O) \simeq +15$ Hz and $\Delta^1J(O,H) \simeq -5$ Hz between the experimental geometry from ref 36 and the equilibrium geometry optimized at the MP2/aug-cc-pVTZ level, in very good agreement with the results obtained in ref 47 with a different functional and a substantially larger basis set (see Table 5.

Table 5. Coupling Constant Variation, Δ^nJ (Hz), Produced by Reasonable Changes in the H_2O_2 Geometry

geometry	change	$\Delta^1J(O,O)$	$\Delta^1J(O,H)$	$\Delta^2J(O,H)$	$\Delta^3J(H,H)$
dihedral angle	10°	3.81	−1.27	−1.08	1.19
angle O−O−H	2°	−2.96	0.07	−0.26	0.20
distance O−H	0.01 Å	−0.36	2.36	0.10	0.07
distance O−O	0.005 Å	1.12	0.40	0.04	−0.01

We find in regards to H_2O_2 coupling constants that geometry effects are more important than environmental effects for $^1J(O,O)$, the environmental influence dominates for $^1J(O,H)$, and both effects are comparable for $^2J(O,H)$. In the case of $^3J(H,H)$, the environmental effects are so tiny that the geometry dependence, although small, dominates.

4. CONCLUDING REMARKS

A sequential procedure using MC simulations and quantum mechanics is used to analyze the effects of solvation on the NMR nuclear shielding and spin−spin coupling constants of hydrogen peroxide in water.

The solute−solvent structure is analyzed in terms of RDFs. The center of mass RDF shows a microsolvation shell around the H_2O_2 of six water molecules. We find that the first peak of $G_{O-H}(r)$, associated with the direct HBs of the solute, appears shifted by −0.06 Å and is more intense for H_2O_2 than that for water in aqueous solution, in agreement with previous work,[38] indicating that H_2O_2 is a better proton donor than water. On the other hand, the intensity of the first peak of $G_{H-O}(r)$ is less intense and displaced by +0.24 Å with respect to the liquid water case, a sign that H_2O_2 is a poorer proton acceptor. Using geometric and energetic criteria, we found an average of 2.8 water molecules hydrogen bonded to the H_2O_2 (0.6 in each hydrogen and 0.8 in each oxygen atom of the H_2O_2). Although, on average, both hydroxyls of the peroxide are equivalent, the distribution of water molecules hydrogen bonded to the H_2O_2 is highly asymmetric. Analyzing the statistics of the HB, we identify that only 34% of the configurations give symmetric distributions, 12% with both hydroxyls acting as the proton donor and 22% with both hydroxyls simultaneously acting as a proton donor and acceptor.

We calculate the magnetic shieldings for hydrogen peroxide in water for 100 solvent configurations that are statistically uncorrelated with the B3LYP/aug-cc-pVTZ level. We find that oxygen gets shielded with respect to the vacuum case (+5.5 ppm) but with large fluctuations from configuration to configuration, while hydrogen is deshielded (−2.9 ppm) and with a smaller spread. The origin of the fluctuations for oxygen are explained in terms of its response when H_2O_2 is hydrogen bonded as a proton donor to a single solvent molecule.

The variation in magnetic shieldings due to the aqueous solution is decomposed in the effect from the first microsolvation shell, explicitly incorporated in the QM treatment (σ_{s+6w}), and the effect from the rest of the liquid, incorporated via the electrostatic field of the atomic point charges of the remaining water molecules (σ_{6w+PC}). We find that the former contribution dominates, although the spread of $\Delta\sigma(O)$ from point charges is substantial. The values for hydrogen are, in ppm, $\sigma_S = 24.2 > \sigma_{S+6W} = 21.8 \pm 0.1 > \sigma_{S+6W+PC} = 21.3 \pm 0.1$ (see section 3.2).

Of the four intramolecular spin−spin coupling constants of the hydrogen peroxide, only the two one-bond constants have a very marked solvent effect, ∼1.6 Hz for $^1J(O,O)$ and ∼14.9 Hz for $^1J(O,H)$. The two-bond couplings have a solvent effect on the order of ∼0.8 Hz, and the remaining one appears to be negligible.

AUTHOR INFORMATION

Corresponding Author

*E-mail: caputo@df.uba.ar. Tel: +54 11 4576-3353. Fax: +54 11 4576-3357.

Notes

The authors declare no competing financial interest.

ACKNOWLEDGMENTS

M.C.C. acknowledges financial support to the present research from CONICET(PIP0369) and Universidad de Buenos Aires (UBACYT,W197); P.F.P. acknowledges financial support from CONICET and UNNE (PI:F002-11 Res.852/11); L.B. acknowledges CIN for the grant BEVC; and S.C., K.C., and H.C.G. acknowledge financial support from CAPES, CNPq, INCT-FCx, and FAPESP (Brazil).

REFERENCES

(1) Kulkarni, A. D.; Pathak, R. K.; Bartolotti, L. J. Structures, Energetics and Vibrational Spectra of $H_2O_2\cdots(H_2O)_n$, n = 1−6 clusters: Ab Initio Quantum Chemical Investigations. *J. Phys. Chem. A* **2005**, *109*, 4583−4590.

(2) Xue-Hai, J.; Ji-Jun, X.; He-Ming, X. Theoretical Study on Intermolecular Interactions and Thermodynamic Properties of Water Hydrogen Peroxide Clusters. *J. Mol. Struct.: THEOCHEM* **2003**, *626*, 231−238.

(3) Ferreira, C.; Martiniano, H. F. M. C.; Cabral, B. J. C.; Aquilanti, V. Electronic Excitation and Ionization of Hydrogen Peroxide−Water Clusters: Comparison with Water Clusters. *Int. J. Quantum Chem.* **2011**, *111*, 1824−1835.

(4) Zhou, Z.; Du, D.; Fu, A. Theoretical Study of the Rotation Barrier of Hydrogen Peroxide in Hydrogen Bonded Structure of HOOH−H_2O Complexes in Gas and Solution Phase. *J. Mol. Struct.: THEOCHEM* **2005**, *717*, 127−134.

(5) Sennikov, P. G.; Ignatov, S. K.; Schrems, O. Complexes and Clusters of Water Relevant to Atmospheric Chemistry: H_2O Complexes with Oxidants. *ChemPhysChem* **2005**, *6*, 392−412.

(6) Kulkarni, A. D.; Pathak, R. K.; Bartolotti, L. J. Effect of Additional Hydrogen Peroxide to $H_2O_2\cdots(H_2O)_n$, n = 1 and 2 Complexes: Quantum Chemical Study. *J. Chem. Phys.* **2006**, *124*, 214309/1−214309/7.

(7) Ignatov, S. K.; Sennikov, P. G.; Jacobi, H. W.; Razuvaev, A. G.; Schrems, O. Surface Species Formed During uv Photolysis of Ozone Adsorbed on Water Ice Films at 80 k. A Combined RAFTIR and DFT Study. *Phys. Chem. Chem. Phys.* **2003**, *5*, 496−505.

(8) Aparicio, F.; Contreras, R.; Galvan, M.; Cedillo, A. Global and Local Reactivity and Activation Patterns of HOOX (X = H, NO_2, CO_2^-, SO_3^-) Peroxides with Solvent Effects. *J. Phys. Chem. A* **2003**, *107*, 10098−10104.

(9) Akiya, N.; Savage, P. E. Effect of Water Density on Hydrogen Peroxide Dissociation in Supercritical Water. 2. Reaction Kinetics. *J. Phys. Chem. A* **2000**, *104*, 4441−4448.

(10) Fedorov, D. G.; Sugita, Y.; Choi, C. H. Efficient Parallel Implementations of QM/MM-REMD (Quantum Mechanical/Molecular Mechanics-Replica-Exchange MD) and Umbrella Sampling: Isomerization of H_2O_2 in Aqueous Solution. *J. Phys. Chem. B* **2013**, *117*, 7996−8002.

(11) de Dios, A. C.; Jameson, C. J. Recent Advances in Nuclear Shielding Calculations. *Annu. Rep. NMR Spectrosc.* **2012**, *77*, 1−80.
(12) Sebastiani, D.; Rothlisberger, U. Nuclear Magnetic Resonance Chemical Shifts from Hybrid DFT QM/MM Calculations. *J. Phys. Chem. B* **2004**, *108*, 2807−2815.
(13) Kongsted, J.; Nielsen, C. B.; Mikkelsen, K. V.; Christiansen, O.; Ruud, K. Nuclear Magnetic Shielding Constants of Liquid Water: Insights from Hybrid Quantum Mechanics/Molecular Mechanics Models. *J. Chem. Phys.* **2007**, *126*, 034510.
(14) Sebastiani, D.; Parrinello, M. A New Ab-Initio Approach for NMR Chemical Shifts in Periodic Systems. *J. Phys. Chem. A* **2001**, *105*, 1951−1958.
(15) Pennanen, T. S.; Vaara, J.; Lantto, P.; Sillanpa, A. J.; Laasonen, K.; Jokisaari, J. Nuclear Magnetic Shielding and Quadrupole Coupling Tensors in Liquid Water: a Combined Molecular Dynamics Simulation and Quantum Chemical Study. *J. Am. Chem. Soc.* **2006**, *126*, 11093−11102.
(16) Mennucci, B.; Tomasi, J. Continuum Solvation Models: A New Approach to the Problem of Solute's Charge Distribution and Cavity Boundaries. *J. Chem. Phys.* **1997**, *106*, 5151−5158.
(17) Coutinho, K.; Canuto, S. Solvent Effects in Emission Spectroscopy: A Monte Carlo Quantum Mechanics Study of the n ← π^* Shift of Formaldehyde in Water. *J. Chem. Phys.* **2000**, *113*, 9132−9139.
(18) Ludwig, V.; Coutinho, K.; Borin, A. C.; Canuto, S. Electronic Polarization of 1H-Benzotriazole in Water: Ground and First Excited-state Dipole Moments. *Int. J. Quantum Chem.* **2003**, *95*, 572−579.
(19) Wolinski, K.; Hilton, J. F.; Pulay, P. Efficient Implementation of the Gauge-Independent Atomic Orbital Method for NMR Chemical Shift Calculations. *J. Am. Chem. Soc.* **1990**, *112*, 8251−60.
(20) Frisch, M. J.; Trucks, G. W.; Schlegel, H. B.; Scuseria, G. E.; Robb, M. A.; Cheeseman, J. R.; Zakrzewski, V. G.; Montgomery, J. A., Jr.; Stratmann, R. E.; Burant, J. C.; et al. *Gaussian03*, revision A.11.2; Gaussian, Inc.: Pittsburgh, PA, 2003.
(21) Becke, A. D. Density-Functional Thermochemistry. III. The Role of Exact Exchange. *J. Chem. Phys.* **1993**, *98*, 5648−5652.
(22) Lee, C.; Yang, W.; Parr, R. G. Development of the Colle−Salvetti Correlation-Energy Formula into a Functional of the Electron Density. *Phys. Rev. B* **1998**, *37*, 785−789.
(23) Krivdin, L. B.; Sauer, S. P. A.; Peralta, J. E.; Contreras, R. H. Non-empirical Calculations of NMR Indirect Carbon−Carbon Coupling Constants: 1. Three-Membered Rings. *Magn. Reson. Chem.* **2002**, *40*, 187−194.
(24) Dunning, T. H., Jr. Gaussian Basis Sets for Use in Correlated Molecular Calculations. I. The Atoms Boron through Neon and Hydrogen. *J. Chem. Phys.* **1989**, *90*, 1007−1023.
(25) Helgaker, T.; Jaszunski, M.; Ruud, K. Ab Initio Methods for the Calculation of NMR Shielding and Indirect Spin−Spin Coupling Constants. *Chem. Rev.* **1999**, *99*, 293−352.
(26) Rusakov, Y. Y.; Krivdin, L. B. Modern Quantum Chemical Methods for Calculating Spin−Spin Coupling Constants: Theoretical Basis and Structural Applications in Chemistry. *Russ. Chem. Rev.* **2013**, *82*, 99−130.
(27) Enevoldsen, T.; Oddershede, J.; Sauer, S. P. A. Correlated Calculations of Indirect Nuclear Spin−Spin Coupling Constants Using Second Order Polarization Propagator Approximations: SOPPA and SOPPA(CCSD). *Theor. Chem. Acc.* **1998**, *100*, 275−284.
(28) Kendall, R. A.; Dunning, T. H.; Harrison, R. J. Electron Affinities of the First-Row Atoms Revisited. Systematic Basis Sets and Wave Functions. *J. Chem. Phys.* **1992**, *96*, 6796−6806.
(29) Provasi, P. F.; Aucar, G. A.; Sauer, S. P. A. The Effect of Lone Pairs and Electronegativity on the Indirect Nuclear Spin−Spin Coupling Constants in CH_2X (X = CH_2, NH, O, S): Ab Initio Calculations Using Optimized Contracted Basis Sets. *J. Chem. Phys.* **2001**, *115*, 1324−1334.
(30) Provasi, P. F.; Sauer, S. P. A. Optimized Basis Sets for the Calculation of Indirect Nuclear Spin−Spin Coupling Constants Involving the Atoms B, Al, Si, P, and Cl. *J. Chem. Phys.* **2010**, *133*, 054308.
(31) Allen, M. P.; Tildesley, D. J. *Computer Simulation of Liquids*; Clarendon: Oxford, U.K., 1987.
(32) Vácha, R.; Slavíček, P.; Mucha, M.; Finlayson-Pitts, B. J.; Jungwirth, P. Adsorption of Atmospherically Relevant Gases at the Air/Water Interface: Free Energy Profiles of Aqueous Solvation of N_2, O_2, O_3, OH, H_2O, HO_2, and H_2O_2. *J. Phys. Chem. A* **2004**, *108*, 11573−11579.
(33) Jorgensen, W. L. Transferable Intermolecular Potential Functions for Water, Alcohols, and Ethers. Application to Liquid Water. *J. Am. Chem. Soc.* **1981**, *103*, 335−340.
(34) Coutinho, K.; Canuto, S. *DICE, A Monte Carlo Program for Molecular Liquid Simulation*; University of São Paulo: São Paulo, Brazil, 2003.
(35) Ichikawaa, K.; Kamedaad, Y.; Yamaguchib, T.; Wakitab, H.; Misawac, M. Neutron-Diffraction Investigation of the Intramolecular Structure of a Water Molecule in the Liquid Phase at High Temperatures. *Mol. Phys.* **1991**, *73*, 79−86.
(36) Redington, R. L.; Olson, W. B.; Cross, P. C. Studies of Hydrogen Peroxide: The Infrared Spectrum and the Internal Rotation Problem. *J. Chem. Phys.* **1962**, *36*, 1311−1326.
(37) Coutinho, K.; Canuto, S.; Zerner, M. C. A Monte Carlo−Quantum Mechanics Study of the Solvatochromic Shifts of the Lowest Transition of Benzene. *J. Chem. Phys.* **2000**, *112*, 9874−9880.
(38) Martins-Costa, M. T. C.; Ruiz-Lopez, M. F. Molecular Dynamics of Hydrogen Peroxide in Liquid Water Using a Combined Quantum/Classical Force Field. *Chem. Phys.* **2007**, *332*, 341−347.
(39) Canuto, S.; Coutinho, K. From Hydrogen Bond to Bulk: Solvation Analysis of the n−π^* Transition of Formaldehyde in Water. *Int. J. Quantum Chem.* **2000**, *77*, 192−198.
(40) Rocha, W. R.; Martins, V. M.; Coutinho, K.; Canuto, S. Solvent Effects on the Electronic Absorption Spectrum of Formamide Studied by a Sequential Monte Carlo/Quantum Mechanical Approach. *Theor. Chem. Acc.* **2002**, *108*, 31−37.
(41) Ramsey, N. F. Electron Coupled Interactions between Nuclear Spins in Molecules. *Phys. Rev.* **1953**, *91*, 303−307.
(42) Lynden-Bell, R. K.; Harris, R. M. *Nuclear Magnetic Resonance Spectroscopy*; Appleton Century Crofts: New York, 1969.
(43) Wigglesworth, R. D.; Raynes, W. T.; Sauer, S. P. A.; Oddershede, J. Calculated Spin−Spin Coupling Surfaces in the Water Molecule; Prediction and Analysis of J(O,H), J(O,D) and J(H,D) in Water Isotopomeres. *Mol. Phys.* **1998**, *94*, 851−862.
(44) Casanueva, J.; San Fabián, J.; Dez, E.; Esteban, A. L. NMR Spin−Spin Coupling Constants in Water Molecule: Equilibrium and Rovibrational Values. *J. Mol. Struct.* **2001**, *565*, 449−454.
(45) Sergeyev, N. M.; Sergeyeva, N. D.; Strelenko, Yu. A.; Raynes, W. T. The 1h-2h, 17o-1h Coupling Constants and the 16o/18o Induced Proton Isotope Shift in Water. *Chem. Phys. Lett.* **1997**, *277*, 142−146.
(46) Kjær, H.; Nielsen, M. R.; Pagola, G. I.; Ferraro, M. B.; Lazzeretti, P.; Sauer, S. P. A. Nuclear Magnetic Resonance J Coupling Constant Polarizabilities of Hydrogen Peroxide: A Basis Set and Correlation Study. *J. Comput. Chem.* **2012**, *33*, 1845−1853.
(47) Alkorta, I.; Elguero, J.; Provasi, P. F.; Ferraro, M. B. Theoretical Study of the 1:1 and 2:1 (Homo- and Heterochiral) Complexes of XOOX′ (X, X′ = H, CH_3) with Lithium Cation. *J. Phys. Chem. A* **2011**, *115*, 7805−7810.
(48) Schäfer, A.; Horn, H.; Ahlrichs, R. Fully Optimized Contracted Gaussian Basis Sets for Atoms Li to Kr. *J. Chem. Phys.* **1992**, *97*, 2571−2578.